# HYDRODYNAMIC FLOW MODELING AT CONFLUENCE OF TWO STREAMS

By K.-H. Wang,[1] T. G. Cleveland,[2] S. Fitzgerald,[3] and X. Ren[4]

**ABSTRACT:** A pseudo three-dimensional (3D), time-dependent hydrodynamic flow model is developed to simulate flood flows at the confluence of Buffalo and White Oak Bayous in Houston, Texas. This model solves Reynolds-averaged Navier-Stokes equations in a curvilinear coordinate system. A simplified moving-boundary algorithm was also incorporated in the model to determine the moving-fluid domain. The 3D velocity field and free-surface elevation at this interconnected bayou system were computed. Numerical simulations were conducted for both existing and proposed channel geometries. Evaluation of the velocity change due to the proposed channel improvements was studied. The effects of the bayou bathymetry and existing structures on the flow field are also discussed.

## INTRODUCTION

The physical behavior of an interconnected riverine system is a complex, dynamic process. It involves the three-dimensional (3D) interaction of the inflow discharges at the confluence. The river geometries, bank roughness, and existing structures all play important roles in influencing the velocity field. The flow-modeling effort can provide important hydraulic information (e.g., velocity, water level, etc.) to assist in the evaluation of the design of the channel improvements.

A one-dimensional (1D) steady approach has been widely used in numerical models for prediction of water level in natural channels (Kraijenhoff and Moll 1986). However, the detailed time variation of velocity distribution, the formation of a turbulent eddy, and the interaction of inflow discharges cannot be evaluated in a 1D steady model. The simulation of steady flow in a rectangular channel near groyne was investigated by Tingsanchali and Maheswaran (1987) using a two-dimensional flow model. Later, Jin and Steffler (1993) presented a depth-averaged finite-element model to predict flow in curved open channels. The 3D flow computation in curved channels with a rectangular cross section or natural bed topography were investigated by Leschziner and Rodi (1979) and Demuren (1993), respectively. However, their models are limited in a steady-state simulation and may not accommodate flow reversal in the main flow direction. The flow-field prediction in a confluence has not yet been studied extensively. A hydraulic geometry relationship-based model for studying changes in channel form at a river confluence was provided by Roy and Woldenberg (1986). The effect of the river-junction condition in flow modeling was discussed by Yen (1979).

In the present study, a pseudo 3D, time-dependent hydrodynamic model with a moving-boundary algorithm was developed to simulate flood flows at the confluence of Buffalo Bayou and White Oak Bayou near downtown Houston. This model solves Reynolds-averaged Navier-Stokes equations in a curvilinear-grid system. The curvilinear-grid model has the advantage of being able to better represent the geometrically complex domain. Important factors such as geometry of confluence, variable depths, bottom stresses, stream inflows, and physiographic features are included. A simplified moving-boundary algorithm was incorporated in the model to update the computational domain. The development of this riverine flow model was essentially based on a 3D hydrodynamic model established by Wang (1994). The 3D velocity field and corresponding water-surface elevation were obtained to describe this bayou system. The study of the velocity impact caused by physiographic or hydrographic changes can be conducted.

In the present study, numerical simulations were conducted for both existing and proposed channel geometries. The design hydrographs of 100 year floods were used as model input for production runs. Velocity fields and water-surface elevations in the existing channel and proposed channel, under different inflow conditions, were generated for comparisons. Water velocities at sensitive cross sections of the bayous and the location of turbulent eddy within the confluence can be determined. Evaluation of the velocity change due to the proposed channel improvements was studied. The effects of the bayou bathymetry and existing structures on the flow field are also discussed.

## BACKGROUND AND STUDY AREA

Fig. 1 shows the confluence of Buffalo Bayou and White Oak Bayou relative to downtown Houston. Flooding and bank erosion at Allen's Landing, where White Oak Bayou meets Buffalo Bayou, are drainage problems that need to be addressed. The Harris County Flood Control District (HCFCD) is planning White Oak Bayou channel improvements by widening the base channel and smoothening the channel bank with concrete pavement. These improvements are primarily designed to convey flood waters more smoothly and efficiently. Reduction of the turbulent eddy in the confluence that is suspected of causing damage to Allen's Landing is a secondary goal of the design. The design considers the historical value of the area, aesthetics, and physical constraints of existing structures. HCFCD improvements in conjunction with a future amenity project will create a setting that will be used as a park during normal flows and will efficiently convey water during storm flows. The hydrodynamic model covers the two bayous from Travis Street on the west side of the confluence to Fannin Street on the east side of the confluence, and from Commerce Street on the south side of the confluence to Main Street Bridge on the north side of the confluence.

The existing digital-terrain map of the study area is shown on Fig. 2. Some geographic features such as streets, bridges, and buildings are also shown on the map for reference. A map of the proposed conditions is shown on Fig. 3. Three typical cross sections (looking downstream) along the White Oak

[1]Assoc. Prof., Dept. of Civ. and Envir. Engrg., Univ. of Houston, Houston, TX 77204-4791.

[2]Assoc. Prof., Dept. of Civ. and Envir. Engrg., Univ. of Houston, Houston, TX.

[3]Mgr., Capital Improvements Dept., Harris County Flood Control Dist., Houston, TX 77092.

[4]Res. Asst., Dept of Civ. and Envir. Engrg., Univ. of Houston, Houston, TX.

Note. Associate Editor: Rene Chevray. Discussion open until March 1, 1997. To extend the closing date one month, a written request must be filed with the ASCE Manager of Journals. The manuscript for this paper was submitted for review and possible publication on January 6, 1995. This paper is part of the ***Journal of Engineering Mechanics***, Vol. 122, No. 10, October, 1996. ©ASCE, ISSN 0733-9399/96/0010-0994–1002/$4.00 + $.50 per page. Paper No. 9880.

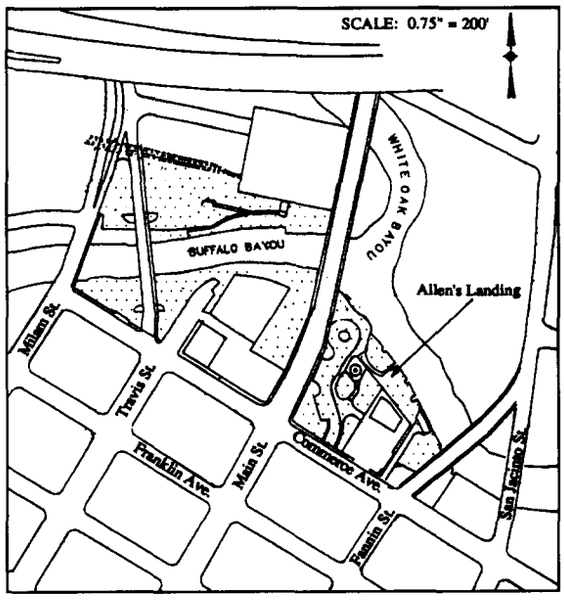


FIG. 1. Study Area—Confluence of Buffalo Bayou and White Oak Bayou

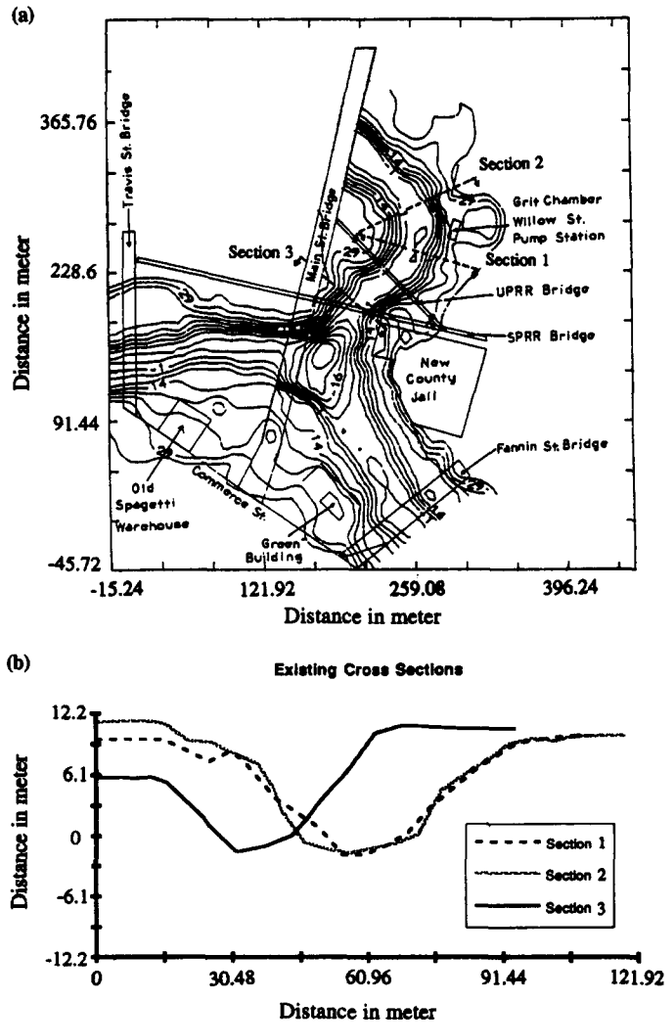


FIG. 2. (a) Topographic Map of Existing Channel Configuration; (b) Selected Cross Sections Plots

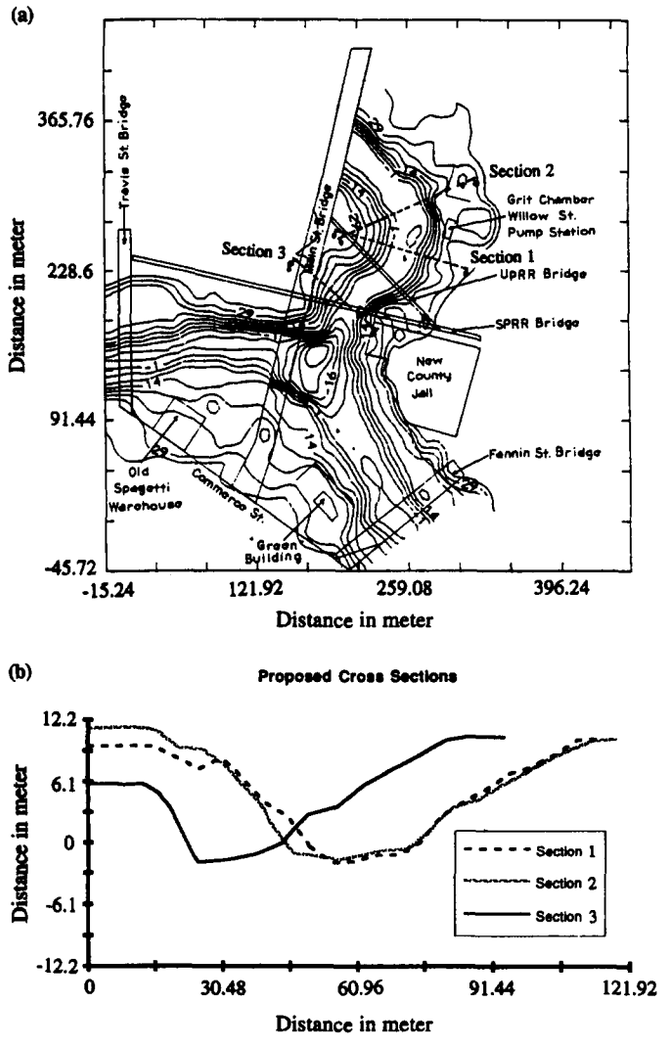


FIG. 3. Plan View: (a) Topographic Map of Proposed Channel Configuration; (b) Selected Cross-Section Plots

Bayou are also plotted as insets in Figs. 2 and 3. Comparing Figs. 2 and 3, White Oak Bayou is changed by widening the base channel and reducing the bank slope. The right bank of White Oak Bayou (looking downstream) near where Main Street crosses Buffalo Bayou is designed to bend toward the confluence region.

## BASIC EQUATIONS AND BOUNDARY CONDITIONS

For this study, a curvilinear pseudo 3D hydrodynamic flow model was developed. The important feature of a moving-fluid domain was simulated in the model. The forcing factors considered in this study are bottom stresses and stream inflows. The basic equations that govern the 3D flow field are Reynolds-averaged Navier-Stokes equations. Using the eddy-viscosity concept, the continuity equation and horizontal momentum equations can be written in Cartesian coordinates as

$$\frac{\partial u}{\partial x} + \frac{\partial v}{\partial y} + \frac{\partial w}{\partial z} = 0 \tag{1}$$

$$\frac{\partial u}{\partial t} + \frac{\partial uu}{\partial x} + \frac{\partial uv}{\partial y} + \frac{\partial uw}{\partial z} = -\frac{1}{\rho}\frac{\partial p}{\partial x} + \frac{\partial}{\partial x}\left(\nu_H \frac{\partial u}{\partial x}\right) + \frac{\partial}{\partial y}\left(\nu_H \frac{\partial u}{\partial y}\right) + \frac{\partial}{\partial z}\left(\nu_V \frac{\partial u}{\partial z}\right) \tag{2}$$

$$\frac{\partial v}{\partial t} + \frac{\partial uv}{\partial x} + \frac{\partial vv}{\partial y} + \frac{\partial vw}{\partial z}$$

$$= -\frac{1}{\rho}\frac{\partial p}{\partial y} + \frac{\partial}{\partial x}\left(\nu_H \frac{\partial v}{\partial x}\right) + \frac{\partial}{\partial y}\left(\nu_H \frac{\partial v}{\partial y}\right) + \frac{\partial}{\partial z}\left(\nu_V \frac{\partial v}{\partial z}\right) \quad (3)$$

The vertical momentum equation is simplified as

$$-(1/\rho)(\partial p/\partial z) = g \quad (4)$$

by assuming a nearly horizontal flow and that the vertical acceleration is negligible compared to the vertical pressure gradient. In these equations, $x$ and $y$ are horizontal coordinates and $z$ points vertically upward; $u$, $v$, and $w$ are velocity components along the $x$-, $y$-, and $z$-directions (Fig. 4), respectively; $\rho$ = fluid density; $g$ = constant of gravitational acceleration; and $\nu_V$ and $\nu_H$ = vertical and horizontal turbulent eddy coefficients, which may vary in time and space.

The boundary conditions for the model are prescribed pressure and stress at the free surface, prescribed shear stress at the fluid-solid interface (bayou bottom and side walls), and prescribed flux at the inflow and outflow boundaries. However, the effect of wind stresses on the free surface are neglected in the present study. The bottom stress-boundary conditions can be computed based on a quadratic stress law

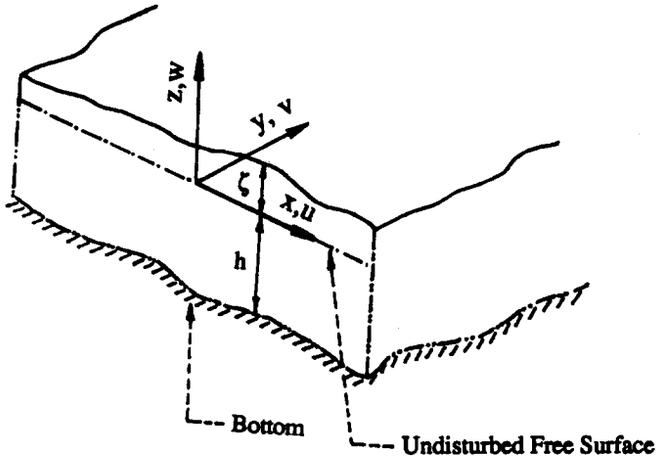


**FIG. 4. Physical Cartesian Coordinate System**

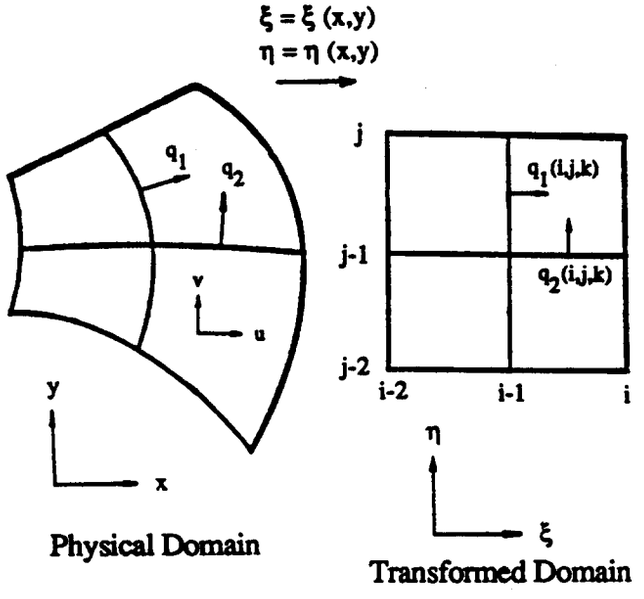


**FIG. 5. Coordinate Transformation and Contravariant Velocity Transformation**

$$\rho\nu_v\left(\frac{\partial u}{\partial z}, \frac{\partial v}{\partial z}\right) = (\tau_{bx}, \tau_{by}) = \rho C_d(u_1^2 + v_1^2)^{1/2}(u_1, v_1) \quad (5)$$

where $C_d$ = drag coefficient; and $u_1$ and $v_1$ = horizontal velocities near the bottom. The drag coefficient is evaluated based on the logarithmic velocity profile near the bottom. Since the channel-bank roughness of the White Oak Bayou is changed considerably after channel improvement, the effect of channel roughness needs to be included in the flow simulation. A simplified bottom-stress formulation was adopted to reflect this effect

$$(\tau_{bx}, \tau_{by}) = \frac{\rho g}{C_c^2}(\bar{U}^2 + \bar{V}^2)^{1/2}(\bar{U}, \bar{V}) \quad (6)$$

where $C_c$ = Chézy coefficient and is given as

$$C_c = H^{1/6}/n \quad (7)$$

where $n$ = Manning's roughness coefficient; $\bar{U}$ and $\bar{V}$ = vertically averaged velocities along the $x$- and $y$-directions, respectively; and $H(x, y, z, t) = h(x, y, z) + \zeta(x, y, t)$ denotes total water depth, where $h$ = undisturbed water depth. With the application of (6), the change of flow field due to the proposed smoother bank along White Oak Bayou can be studied. The normal velocity component is prescribed at the upstream inflow boundaries, and the normal velocity gradient is assumed to be zero at the downstream outflow boundary.

## TRANSFORMED EQUATIONS AND BOUNDARY CONDITIONS

A curvilinear coordinate-transformation technique (Thompson and Johnson 1985) has been used to develop this curvilinear-grid model to minimize the number of grid points and to better represent the geometrically complex flow domains and bathymetry. A vertically dilated coordinate or $\sigma$-grid (Phillips 1957; Sheng et al. 1990), namely

$$\sigma = (z - \zeta)/H \quad (8)$$

was adopted to resolve bathymetry and vertical grids gradually. To further facilitate the applications of the boundary conditions at the lateral fluid-solid interface, Cartesian velocity components $u$ and $v$ in the $x$- and $y$-directions are also transformed into contravariant velocities $q_1$ and $q_2$ by

$$q_1 = \xi_x u + \xi_y v = \frac{y_\eta}{J} u - \frac{x_\eta}{J} v \quad (9a)$$

$$q_2 = \eta_x u + \eta_y v = \frac{-y_\xi}{J} u + \frac{x_\xi}{J} v \quad (9b)$$

where $q_1$ and $q_2$ are perpendicular to the $\eta$ and $\xi$ lines, as shown in Fig. 5, respectively. The subscripts of $\xi_x$, $\eta_x$, $\xi_y$, $\eta_y$, $y_\eta$, $x_\eta$, $y_\xi$, and $x_\xi$ denote partial differentiation. The vertical velocity along the $\sigma$-direction is defined by $\omega$, where $\omega = d\sigma/dt$.

Using the free-surface kinematics

$$\frac{\partial \zeta}{\partial t} + u\frac{\partial \zeta}{\partial x} + v\frac{\partial \zeta}{\partial y} = w \quad (10)$$

and applying these transformations of the coordinates and velocity fields, the 3D equations of motion written in terms of the horizontal contravariant velocity components ($q_1$, $q_2$) and vertical velocity $\omega$ in the transformed coordinates ($\xi$, $\eta$, $\sigma$) were derived as

$$\frac{\partial \zeta}{\partial t} + \frac{1}{J}\left[\frac{\partial}{\partial \xi}(JHq_1) + \frac{\partial}{\partial \eta}(JHq_2)\right] + H\frac{\partial \omega}{\partial \sigma} = 0 \quad (11)$$

$$\frac{1}{H}\frac{\partial Hq_1}{\partial t} = -g\left(\mathbf{g}^{11}\frac{\partial \zeta}{\partial \xi} + \mathbf{g}^{12}\frac{\partial \zeta}{\partial \eta}\right) - \frac{1}{HJ^2}\left\{y_\eta\left[\frac{\partial}{\partial \xi}(x_\xi HJq_1^2 + x_\eta HJq_1q_2) + \frac{\partial}{\partial \eta}(x_\xi HJq_1q_2 + x_\eta HJq_2^2)\right] - x_\eta\left[\frac{\partial}{\partial \xi}(y_\xi HJq_1^2 + y_\eta HJq_1q_2) + \frac{\partial}{\partial \eta}(y_\xi HJq_1q_2 + y_\eta HJq_2^2)\right] + J^2\frac{\partial Hq_1\omega}{\partial \sigma}\right\} + \frac{1}{H^2}\frac{\partial}{\partial \sigma}\left(\upsilon_v\frac{\partial q_1}{\partial \sigma}\right) + \upsilon_H(\text{horizontal diffusion of } q_1) \tag{12}$$

$$\frac{1}{H}\frac{\partial Hq_2}{\partial t} = -g\left(\mathbf{g}^{21}\frac{\partial \zeta}{\partial \xi} + \mathbf{g}^{22}\frac{\partial \zeta}{\partial \eta}\right) - \frac{1}{HJ^2}\left\{-y_\xi\left[\frac{\partial}{\partial \xi}(x_\xi HJq_1^2 + x_\eta HJq_1q_2) + \frac{\partial}{\partial \eta}(x_\xi HJq_1q_2 + x_\eta HJq_2^2)\right] + x_\xi\left[\frac{\partial}{\partial \xi}(y_\xi HJq_1^2 + y_\eta HJq_1q_2) + \frac{\partial}{\partial \eta}(y_\xi HJq_1q_2 + y_\eta HJq_2^2)\right] + J^2\frac{\partial Hq_2\omega}{\partial \sigma}\right\} + \frac{1}{H^2}\frac{\partial}{\partial \sigma}\left(\upsilon_v\frac{\partial q_2}{\partial \sigma}\right) + \upsilon_H(\text{horizontal diffusion of } q_2) \tag{13}$$

In (11)–(13), $J = x_\xi y_\eta - x_\eta y_\xi$ is the Jacobian of transformation; and $\mathbf{g}^{ij}$ denotes the conjugate metric tensors (see Appendix I). The complete expressions of horizontal diffusion terms in (12) and (13) are described in Wang (1994).

The computation of the unknown $\zeta$ can be decoupled from the 3D equations by a mode-splitting technique. This technique permits the external free-surface elevation to be calculated from the vertically integrated equations. The vertically integrated equations are obtained by integrating the 3D momentum equations [(11)–(13)] from the bottom to the free surface and are given as

$$\frac{\partial \zeta}{\partial t} + \frac{1}{J}\left[\frac{\partial}{\partial \xi}(JU) + \frac{\partial}{\partial \eta}(JV)\right] = 0 \tag{14}$$

$$\frac{\partial U}{\partial t} + Hg\left(\mathbf{g}^{11}\frac{\partial \zeta}{\partial \xi} + \mathbf{g}^{12}\frac{\partial \zeta}{\partial \eta}\right) = F(\xi, \eta) \tag{15}$$

$$\frac{\partial V}{\partial t} + Hg\left(\mathbf{g}^{21}\frac{\partial \zeta}{\partial \xi} + \mathbf{g}^{22}\frac{\partial \zeta}{\partial \eta}\right) = G(\xi, \eta) \tag{16}$$

where $F(\xi, \eta)$ and $G(\xi, \eta)$ represent the vertically integrated, nonlinear and diffusion terms and bottom stresses from (12) and (13), respectively. The vertically integrated velocities $U$ and $V$ are defined as

$$(U, V) = H\int_{-1}^{0}(q_1, q_2)\, d\sigma \tag{17}$$

## NUMERICAL METHOD

The numerical approach is based on a three-time-level implicit finite-difference scheme. A staggered grid is used in both the horizontal and vertical directions of the computational domain. The mode-splitting technique is applied to permit the computation of the external free-surface elevation to be decoupled from the 3D equations. The external mode of the flow, which is described by the free-surface elevation and vertically integrated currents, can be calculated from the vertically integrated equations [(14)–(16)] by using the alternating-direction-implicit method (see Wang et al. 1991).

Defining velocity deficits as $\tilde{q}_1 = q_1 - \bar{q}_1$ and $\tilde{q}_2 = q_2 - \bar{q}_2$, where $\bar{q}_1 = U/H$ and $\bar{q}_2 = V/H$, we obtain the differential equations for the internal mode computation by subtracting the vertically integrated momentum equations from the 3D momentum equations

$$\frac{1}{H}\frac{\partial H\tilde{q}_1}{\partial t} = BX - \frac{F}{H} + \frac{1}{H^2}\frac{\partial}{\partial \sigma}\left(\upsilon_v\frac{\partial \tilde{q}_1}{\partial \sigma}\right) \tag{18}$$

$$\frac{1}{H}\frac{\partial H\tilde{q}_2}{\partial t} = BY - \frac{G}{H} + \frac{1}{H^2}\frac{\partial}{\partial \sigma}\left(\upsilon_v\frac{\partial \tilde{q}_2}{\partial \sigma}\right) \tag{19}$$

where $BX$ and $BY$ represent every term (except vertical diffusion terms and free-surface gradient terms) on the right side of (12) and (13), respectively.

For solving $\tilde{q}_1$ and $\tilde{q}_2$, the vertical diffusion terms in (18) and (19) are treated implicitly to ensure numerical stability. The contravariant velocities are calculated and then transformed back to the physical-velocity components for analyses. The vertical velocity $\omega$ is determined from transformed (11) as

$$\omega = -\frac{1+\sigma}{H}\frac{\partial \zeta}{\partial t} - \frac{1}{H}\int_{-1}^{\sigma}\frac{1}{J}\left[\frac{\partial}{\partial \xi}(JHq_1) + \frac{\partial}{\partial \eta}(JHq_2)\right]d\sigma \tag{20}$$

The physical vertical-velocity component $w$ can then be obtained from

$$w = H\omega + (1+\sigma)\frac{d\zeta}{dt} + \sigma\left(q_1\frac{\partial h}{\partial \xi} + q_2\frac{\partial h}{\partial \eta}\right) \tag{21}$$

The present code allows the vertical turbulent eddy coefficients $\upsilon_v$ to be determined from a simplified second-order turbulence closure model (Donaldson 1973; Sheng et al. 1990). Under the assumption of local equilibrium, this simplified second-order closure model is formulated by neglecting the evolution and diffusion terms from the full Reynolds stress equations. A coupled set of algebraic, equilibrium equations are solved to obtain the Reynolds stress correlations and the total RMS turbulent velocity $q$. The vertical eddy viscosity is then computed from $\upsilon_v = (1 - 2b)\Lambda q/3$. Length scale $\Lambda$ is assumed to be a linear function of vertical distance immediately above the bottom or below the free surface. The invariant model constant $b$ has the value 0.125 (Sheng et al. 1990).

## MOVING-BOUNDARY ALGORITHM

To study the 3D flow interaction and turbulent recirculation at the confluence of Buffalo Bayou and White Oak Bayou, a moving-boundary algorithm was developed and included in the hydrodynamic model to simulate the moving-fluid domain. When both Buffalo Bayou and White Oak Bayou convey their base flows or small discharge flows, the flow regions are defined in the base channels. Most of the banks and floodplain are dry, and no flow exists in these areas. Once the storm water discharges into the bayous, water surface rises up and wets a large area. The model assumes that the flow region is expanded by floodwater, and an expanded computational domain is then required for simulation. In the recession stage of the flood flow, the discharge decreases and water surface drops down. The current hydrodynamic model includes the capability of handling this moving-boundary feature to simulate the flow field in the entire wetted area. The actual velocity field and water level in both bayous due to the continuous flood inputs can be determined.

To accomplish the simulation of a moving-boundary flow region, the maximal region that is expected to be wetted by the design flood is first specified. In this study, expected flow fields using 100 year flood hydrographs were selected for this purpose. A physical boundary based on the existing structures and bottom elevation of 10.973 m (36 ft) (relative to the mean seawater level) was defined as the maximal extent of flow. The

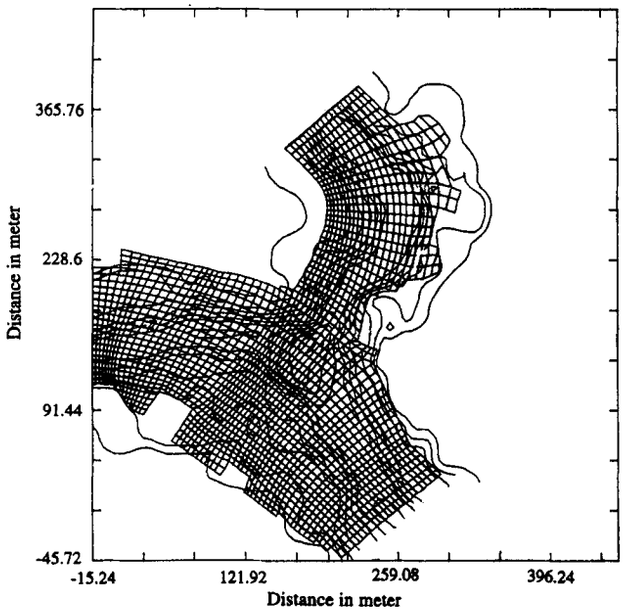


**FIG. 6. Curvilinear Grid System for Confluence of Buffalo and White Oak Bayou**

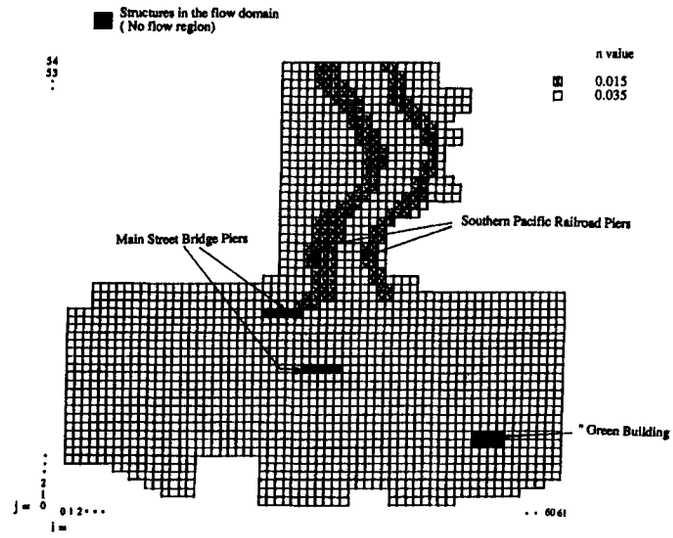


**FIG. 7. Computational Domain and Manning's *n* Values**

domain inside this area is considered as a possible wet area. The domain outside this boundary is a no-flow zone for the entire simulation. Using this defined boundary, the curvilinear grids for hydrodynamic simulation were generated and plotted in Fig. 6. The detailed description of the grid generation is given in Wang et al. (1991). This computational domain is selected to cover the confluence and immediate upstream and downstream of two streams.

The elevation of the channel bottom at each grid point can be determined based on the bayou geometry data. These inputted bottom elevations are used in the model to evaluate the water depth. If the channel bottom is below the free-surface elevation, the water depths in the bayou domain are obtained by subtracting the elevation of the channel bottom from the surface elevation. This water depth is then used as a reference to determine whether an adjacent grid point needs to be modeled as a dry cell or as a wet cell. Once the free-surface elevation rises above the bottom elevation of an adjacent dry cell along the banks, the dry cell is redefined as a wet cell. The flow simulation then continues using the newly defined computational domain. The procedure to test the wet area is repeated, and the next flow boundary is generated. This moving-fluid domain can be clearly observed in the velocity vector plots presented in the results section.

## NUMERICAL SIMULATION

The entire dynamic effect of the flow field at confluence due to the time-varying inflow discharge is simulated using the present hydrodynamic model. This flow model has been tested and calibrated in several water domains (Wang 1992; Wang 1994). From these studies, the model predictions agree fairly well with the measured data. In the present study, the base-flow simulation also agrees reasonably well with the observed flow field.

Fig. 6 shows the curvilinear-grid system of the study area (100 year floodplain). The corresponding computational domain is shown in Fig. 7. The 100 year storm-induced flood flows were inputted at upstream boundaries for simulation. The hydrographs of both bayous are shown in Fig. 8.

To examine the variation of flow field under various inflow conditions, we have selected three inflow conditions for model simulations. These include a 100 year flood from both bayous, a 100 year flood from White Oak Bayou and base flow from Buffalo Bayou (56.63 $m^3/s$), and a 100 year flood from Buffalo Bayou and base flow (70.8 $m^3/s$) from White Oak Bayou. Computations were also conducted for both existing and proposed channels for comparisons. Fig. 8 depicts the relationship between the simulation hour and hydrograph hour. All the results shown in this paper are given in simulation hours. The overall simulations performed were: case a, 28 h of continuous simulation from hydrograph hour 8 to hour 36; case b, 18 h of simulation from hydrograph hour 7 to hour 25; and case c, 28 h of continuous flood discharges from hydrograph hour 7 to hour 35.

These discharge inputs were selected to range from the starting low flow to peak flow then back to low flow, so that the continuous dynamic effect of flood flow could be studied for various flow conditions on each bayou. Even though 100 year hydrographs were used, the dynamic simulation covers the full range of flood frequencies from base discharge to 100 year discharge.

The fluid flow in the bayous is greatly influenced by the bottom stresses. Manning's $n$ values were included in the model to compute bottom stresses. To simulate the flow field in the existing condition, Manning's roughness coefficients were specified as 0.035 for the entire computational domain. However, for the proposed channels, a distribution of Manning's $n$ values (as shown in Fig. 7) was used. The $n$ values of the cells marked with the "x" symbol were 0.015 while the $n$ values of the remaining cells were 0.035. This proposed channel reflects a smoother bank along the White Oak Bayou. The time step used for model simulation is 6 s. In the following section, the interesting results under combined inflows and White Oak dominant inflows at selected time instants are discussed.

## RESULTS

This modeling effort evaluated the hydraulic efficiency and flow condition for the designed channel. First, the flow field at either existing or proposed bayou geometry under inflow conditions of 100 year flood from both bayous are presented. The predicted velocity distribution in the existing channel is compared with the velocity field obtained in the proposed channel. The velocity magnitude and orientation in the flow region is depicted on the velocity vector plots. The contour maps and geographic features of streets, bridges, and buildings are also included on the vector plots to assist in physical interpretation.

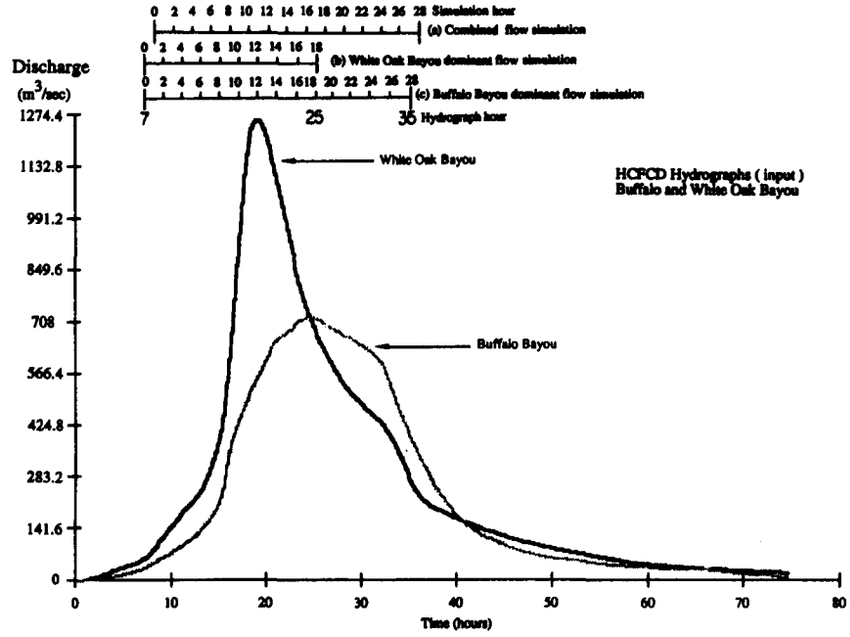


**FIG. 8. 100 yr Flood Hydrographs for Buffalo and White Oak Bayou**

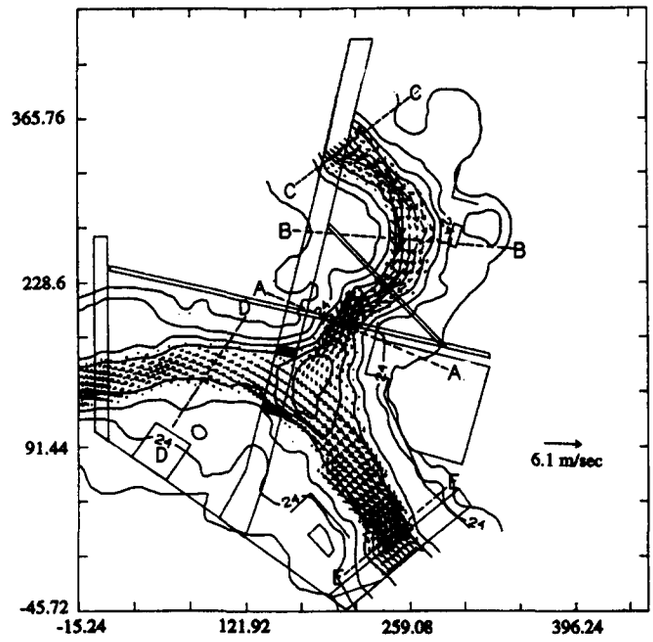


**FIG. 9. Surface-Velocity Field for Existing Channel at $t$ = 6 h under Combined Inflows**

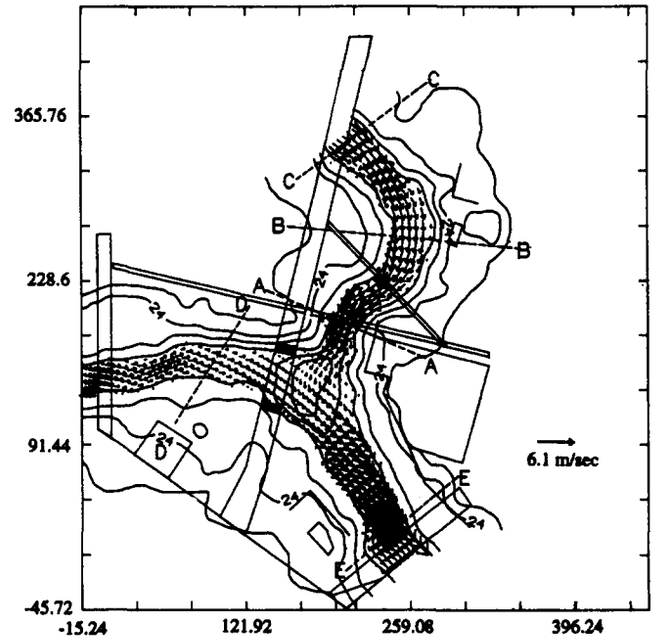


**FIG. 10. Surface-Velocity Field for Proposed Channel at $t$ = 6 h under Combined Inflows**

The velocity field near the water surface (top) of the existing channel at $t$ = 6 h is shown in Fig. 9. At this early stage of simulation (rising limb of input hydrograph), the flow is basically contained in the normal stream channels. The surface fluid velocities along White Oak Bayou in the existing channel range from 0.05 to 3.7 m/s. Abrupt changes in velocity magnitude and flow direction can be observed in the existing channel, especially around the bend of White Oak Bayou where the model predicts the potential formation of a turbulent recirculating eddy. The flow path of White Oak Bayou as it approaches the confluence is nearly perpendicular to the downstream flow direction of Buffalo Bayou. At the bottom layer, the velocities range from 0.037 to 1.84 m/s. In general, the flow fields along the bayou bottom have the same flow pattern as the surface flow fields, but with smaller magnitude.

The surface velocity vector plot for the proposed channel at $t$ = 6 h is presented in Fig. 10. From Fig. 10, it is found that the proposed channel configuration leads to a smoother flow field, and the potential turbulent eddy around the bend of White Oak Bayou is no longer apparent. The flow velocities along White Oak Bayou in the proposed channel range from 0.12 to 1.88 m/s in the bottom layer and from 0.183 to 3.61 m/s in the surface layer. Over an entire section, the average velocity magnitude in the proposed channel is slightly larger than that in the existing channel because the banks of the proposed channel are relatively smoother. The higher velocities allow more discharge to pass a point at the same water-surface elevation. The potential for increased scour is mitigated by the fact that these hydraulically smoother channels are paved with concrete, which will have greater resistance to erosion than the existing natural channel material.

The velocity fields at the recession stage ($t$ = 18 h) are

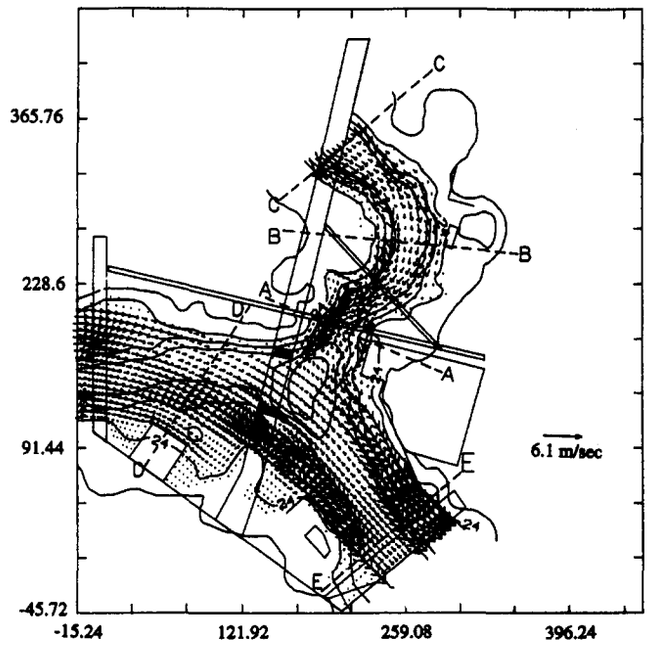


**FIG. 11. Surface-Velocity Field for Existing Channel at $t = 18$ h under Combined Inflows**

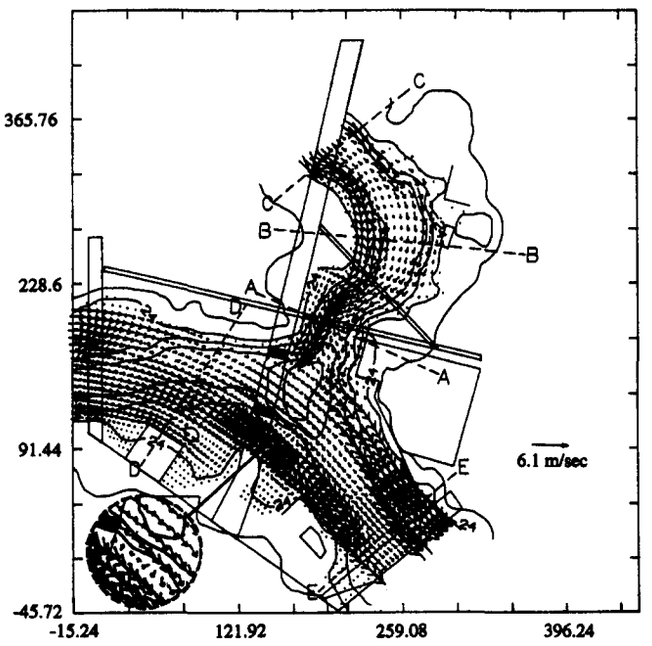


**FIG. 12. Surface-Velocity Field for Proposed Channel at $t = 18$ h under Combined Inflows**

shown in Figs. 11 and 12 for existing and proposed channels, respectively. The model boundary is extended beyond the normal bayou channels, reflecting the increased water-surface area and depth associated with flood flow at these discharges. The uniformity of the velocity field patterns is still evident in the proposed White Oak Bayou simulation. It is interesting to note a recirculation zone is formed right behind the south pier of the main street bridge in the proposed condition (see the enlarged local velocity vector plot). Although this recirculating eddy flow may result in bank erosion, the magnitude of the velocities in the wake of the bridge is smaller in the proposed configuration.

It is also found that, even during the stage of peak flow from White Oak Bayou, a smoother flow pattern is still observed along the proposed White Oak Bayou. The velocity field suggests that the improved channel conveys the flood discharge more efficiently and smoothly. It is interesting to note that the flow field along Allen's landing has smaller bottom velocities in the proposed conditions than those in the existing conditions, suggesting that the proposed design turns the flow from White Oak Bayou towards the downstream boundary of Fannin Street Bridge.

Simulations using an input hydrograph of 100 year flood flow from White Oak Bayou and a steady base flow of 56.63 $m^3/s$ (2,000 cfs) from Buffalo Bayou were also conducted for both the existing and proposed channel configurations. During the initial low flow rates, the flow is contained in the normal stream channels. The predicted velocity field in the existing and proposed channels is presented, respectively, in Figs. 13 and 14 ($t = 4$ h). The results indicate that a more uniform flow field pattern is again displayed in the proposed channel configuration. As inflow discharge increases, the velocity fields

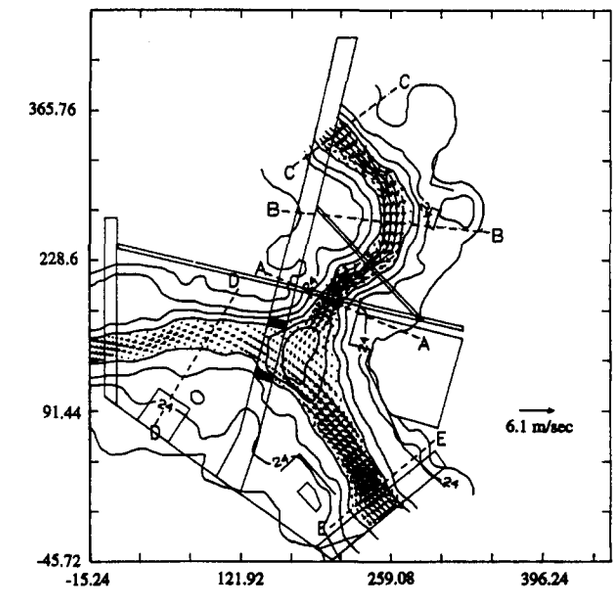


**FIG. 13. Surface-Velocity Field for Existing Channel at $t = 4$ h under White Oak Dominant Inflow**

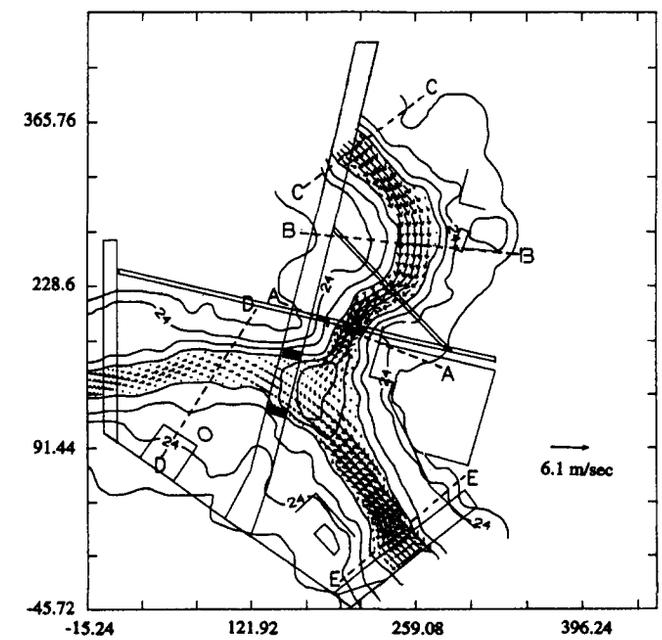


**FIG. 14. Surface-Velocity Field for Proposed Channel at $t = 4$ h under White Oak Dominant Inflow**

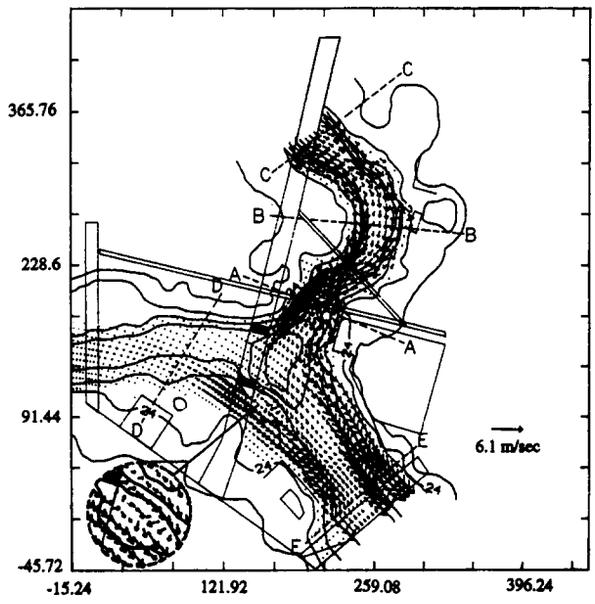


**FIG. 15. Surface-Velocity Field for Existing Channel at $t = 18$ h under White Oak Dominant Inflow**

increase uniformly in the proposed channel, and the flood flow is routed downstream more efficiently and smoothly than in the existing channel. The flow field pattern at the downstream Buffalo Bayou boundary is mainly influenced by the flow from White Oak Bayou. In this White Oak dominant-flow simulation, a portion of flow from White Oak Bayou impacts on the south pier of the Main Street Bridge and Allen's Landing area, but the bulk of the flood flow from White Oak Bayou is simply turned downstream toward the Fannin Street Bridge at the confluence area.

A distinct recirculation is depicted in the wake of the south pier of the Main Street Bridge at $t = 18$ h for both the existing and proposed channels. This recirculation flow pattern is shown in Fig. 15. Again, the magnitude of velocities in the wake of the south pier of the Main Street Bridge are smaller for the proposed conditions.

Simulations using an input hydrograph of 100 year flood flow for Buffalo Bayou and a steady base flow of 70.8 $m^3/s$ (2,500 cfs) from White Oak Bayou were also conducted for both the existing and proposed channels. Since the proposed configuration is mainly focused on improving White Oak Bayou, the computed velocity field for either existing or proposed configurations are practically indistinguishable from each other. It is interesting to point out that no recirculation current is formed at the south pier of the Main Street Bridge in these Buffalo Bayou dominant simulations. This prediction indicates that the contribution of flow from White Oak Bayou plays an important role in generating recirculating currents in the wake of the south pier of the Main Street Bridge.

## CONCLUSION

A 3D hydrodynamic model that used bayou inflows, bayou geometry, and bottom stresses to compute the time-varying velocity field and free-surface elevation was applied to the confluence of Buffalo Bayou and White Oak Bayou. A moving-boundary algorithm was also developed and included in the flow model to simulate the moving-fluid domain. Numerical simulations were conducted for both existing and proposed channel geometries. Design hydrographs of 100 year floods were used as hydrologic inputs. Velocity fields in the existing channel and proposed channel, under different inflow conditions, were generated for comparisons. Interpretation of model results indicate that the proposed bayou modifications studied will convey White Oak flood waters more smoothly. This hydrodynamic flow model is demonstrated to be a useful engineering tool to predict the velocity field in a riverine system.

## ACKNOWLEDGMENTS

This work was sponsored by the Harris County Flood Control District under the University of Houston contract 0279154. The views, opinions, and/or findings contained in this paper are those of the writers and do not represent the position, policy, or decision of the Harris County Flood Control District.

## APPENDIX I.

Expressions of metric tensors include the following:

$$\mathbf{g}^{22} = \mathbf{g}_{11}/J^2; \quad \mathbf{g}^{11} = \mathbf{g}_{22}/J^2 \tag{22a,b}$$

$$\mathbf{g}^{12} = \mathbf{g}^{21} = -\mathbf{g}_{12}/J^2; \quad \mathbf{g}_{22} = x_\eta^2 + y_\eta^2 \tag{22c,d}$$

$$\mathbf{g}_{11} = x_\xi^2 + y_\xi^2; \quad \mathbf{g}_{12} = \mathbf{g}_{21} = x_\xi x_\eta + y_\xi y_\eta \tag{22e,f}$$

## APPENDIX II. REFERENCES

Demuren, A. O. (1993). "A numerical model for flow in meandering channels with natural bed topography." *Water Resour. Res.*, 29(4), 1269–1277.

Donaldson, C. duP. (1973). "Atmospheric turbulence and the dispersal of atmospheric pollutants." *AMS workshop on micrometeorology*, D. A. Haugen, ed., Science Press, Boston, Mass., 313–392.

Jin, Y. C., and Steffler, P. M. (1993). "Predicting flow in curved open channels by depth-averaged method." *J. Hydr. Engrg.*, ASCE, 119(1), 109–124.

Kraijenhoff, D. A., and Moll, J. R. (1986). *River flow modelling and forecasting*. D. Reidel Publishing Company, Dordrecht, The Netherlands.

Leschziner, M. A., and Rodi, W. (1979). "Calculation of strongly curved open channel flow." *J. Hydr. Engrg.*, ASCE, 105(10), 1297–1314.

Phillips, N. A. (1957). "A coordinate system having some special advantages for numerical forecasting." *J. Meteorology*, 14(2), 184–185.

Roy, A. G., and Woldenberg, M. J. (1986). "A model for changes in channel form at a river confluence." *J. Geol.*, 94, 402–411.

Sheng, Y. P., Choi, J. K., and Kuo, A. Y. (1990). "Three-dimensional numerical modeling of tidal circulation and salinity transport in James River Estuary." *Proc., Estuarine and Coast. Modeling*, ASCE, New York, N.Y., 209–218.

Thompson, J. F., and Johnson, B. H. (1985). "Development of an adaptive boundary-fitted coordinate code for use in coastal and estuarine areas." *Tech. Rep. HL-85-5*, U.S. Army Engineer Waterways Experiment Station, Vicksburg, Miss.

Tingsanchali, T., and Maheswaran, S. (1987). "2-D depth-averaged flow computation near groyne." *J. Hydr. Engrg.*, ASCE, 116(1), 71–86.

Wang, K. H., Cleveland, T. G., Rogers, J. R., and Ren, X. (1991). "A three-dimensional hydrodynamic flow and transport model of the confluence of Buffalo Bayou and White Oak Bayou in Houston, Texas—theory, numerical implementation, and results." *Final Rep., Univ. of Houston, UH-CEE91-7, Houston, Tex.*

Wang, K. H. (1992). "Three-dimensional circulation modeling of the coastal and ocean environments." *Civ. Engrg. in the Oceans V Conf.*, ASCE, New York, N.Y., 637–651.

Wang, K. H. (1994). "Characterization of circulation and salinity change in Galveston Bay." *J. Engrg. Mech.*, ASCE, 120(3), 557–579.

Yen, B. C. (1979). "Unsteady flow mathematical modeling techniques." *Modeling of rivers*, H. W. Shen, ed., John Wiley and Sons, Inc., New York, N.Y.

## APPENDIX III. NOTATION

*The following symbols are used in this paper:*

$g$ = gravitational constant;
$\mathbf{g}_{ij}$ = metric tensors;
$g^{ij}$ = conjugate metric tensors;
$H$ = total water depth;
$J = x_\xi y_\eta - x_\eta y_\xi$;
$p$ = pressure distribution;

$q_1, q_2$ = contravariant velocities;
$\tilde{q}_1 = q_1 - \bar{q}_1$;
$\bar{q}_1 = U/H$;
$\tilde{q}_2 = q_2 - \bar{q}_2$;
$\bar{q}_2 = V/H$;
$U$ = vertically integrated velocity along $x$-direction;
$u$ = velocity along $x$-direction;
$V$ = vertically integrated velocity along $y$-direction;
$v$ = velocity along $y$-direction;
$w$ = velocity along $z$-direction;
$x, y, z$ = Cartesian coordinates;
$\zeta$ = free-surface elevation;
$\eta$ = horizontal curvilinear coordinates;
$\Lambda$ = turbulent length scale;
$\xi$ = horizontal curvilinear coordinates;
$\rho$ = fluid density;
$\sigma$ = vertically dilated coordinate [see Eq. (9)];
$\tau_{bx}$ = bottom stress along $x$-direction;
$\tau_{by}$ = bottom stress along $y$-direction;
$\upsilon_H$ = horizontal diffusion coefficient;
$\upsilon_V$ = vertical turbulent eddy coefficient; and
$\omega$ = vertical velocity along $\sigma$-direction.